showed favorable properties for cell growth.

Cell proliferation

The number of cells that proliferated on CNTs was larger than on PC and GP. SW in particular showed near confluence at 7 days and the largest proliferation rate from 3 to 7 days. Cell proliferation is influenced by surface characteristics such as topography[29] and the chemical state[30,31]. A nanoporous structure was found to provide a favorable surface architecture for osteoblast function[32]. In this study, the large number of attached cells on CNT scaffolds could be attributed to the nanostructures with high porosity and a specific surface area.

Protein adsorption on scaffolds

CNTs have the ability to adsorb various molecules non-specifically[33,34]. As it is very likely that adsorbed proteins in serum influence the properties for cell proliferation and growth, protein adsorption on the scaffolds was evaluated in this study. Adsorption of proteins was higher on SW than on other substrates. Therefore, in addition to surface topography, this might further enhance cell proliferation and growth. For GP, its nonthrombogenic property made it difficult for various molecules to be adsorbed on the surface, and thus it is used for heart valve prosthetics[35]. As a result, although both CNTs and GP consisted of carbon, their cell responses were quite different. On CNTs with the surface modified by various proteins and other molecules, cell proliferation and growth were easier. This was a chief reason why cell proliferation and growth were excellent on SW.

Cell functions

The functional activity of proliferated cells and its dependence on scaffolds were evaluated by measuring the ALP activity, which is the most commonly used markers for bone formation of osteoblast cells[36]. Total ALP was the whole amount synthesized by the cells proliferated on the scaffolds. Normalized ALP activity was expressed as activity per unit protein, which could compare qualitatively the degree of activity for each scaffold system. According to the normalized ALP activity (Fig. 6), cells on GP were inert with respect to bone formation, while those on CNTs had high activity. Further, cell proliferation on SW was higher than on MW (Fig. 4). From the results on the number of cells cultured (Fig. 4) and total ALP activity (Fig. 5), cell function per cell on MW was higher than that on SW. These results thus further indicated that proliferation and ALP activity were expected to follow trends of lower proliferation and increased ALP production for porous scaffold[37].

Origin of biocompatibility of CNTs

The present study investigated the cellular response of osteoblasts to various carbon materials: GP, MW, and SW. On CNTs there was efficient cell proliferation and function, whereas there was very little on GP. Cellular response depends on the chemical properties of the substrate, and CNT surface can be modified with various molecules. In the present case, proteins in culture medium were adsorbed on CNTs but very minimally so on GP, as seen in Fig. 3. Our previous study also showed that apatite was precipitated on CNTs when they were immersed in a simulated body fluid[33]. Taken together, the different surface chemical properties between CNTs and GP might originate or stem from their different crystal structures. As a result, although both CNTs and GP were composed of graphene sheets, they demonstrate different affinities toward proteins.

In addition, CNT scaffolds had a high specific surface area due to the small diameter of the CNTs and the porosity of the network structure. As a result, culture medium was easily soaked into the dense meshwork nanostructure formed by the CNTs. In other words, uptake of nutrition and molecules necessary for the extracellular matrix for cell adhesion and growth could be easily done through the mesh-like structure. These factors then led to the high cell adhesion, proliferation, spreading, and growth of filopodia on CNTs.

Carbon as a raw material is originally bioinert in terms of its chemical properties. The topological features of the nanonetwork assembly and the surface modification by apatite precipitation and protein adsorption served to convert CNTs into a bioactive material with pronounced cell proliferation and functional activities.

CONCLUSIONS

Although GP, MW, and SW were isomorphs composed only of carbon atoms, their osteoblast cell responses in terms of cell morphology, cell proliferation, and ALP activity were quite different. With CNTs, cell growth, proliferation, and functions were higher than GP. In particular, cell proliferation and total ALP activity on SW were higher than on MW. These results could be due to the surface topology and chemical properties of the substrates. The former was the dense meshwork nanostructure of CNTs. The latter was the protein adsorption on CNT surface in the cell culture medium. Together, these properties made the CNTs well poised as scaffold materials for cell culture.

ACKNOWLEDGEMENTS

This research was supported in part by Health and

Labor Sciences Research Grants for Research on Chemical Substance Assessment from the Ministry of Health, Labor and Welfare, Japan (H18-Chemistry-General-006), and by Grants (Nos. 16390549 and 17659602) from the Ministry of Education, Sports, Science and Technology, Japan.

REFERENCES

1) Feynman R. There's plenty of room at the bottom. Science 1991; 254:1300-1301.
2) Siegel RW. Creating nanophase materials. Sci Am 1996; 275:42-47.
3) Labhasetwar V. What is next for nanotechnology? J Biomed Nanotechnol 2005; 1:373-374.
4) Park GE, Webster TJ. A review of nanotechnology for the development of better orthopedic implants. J Biomed Nanotechnol 2005; 1:18-29.
5) Iijima S. Helical microtubules of graphitic carbon. Nature 1991; 354:56-58.
6) Uo M, Tamura K, Sato Y, Yokoyama A, Watari F, Totsuka Y, Tohji K. The cytotoxicity of metal-encapsulating carbon nanocapsules. Small 2005; 1:816-819.
7) Harrison BS, Atala A. Carbon nanotube applications for tissue engineering. Biomaterials 2007; 28:344-353.
8) Chlopek J, Czajkowska B, Szaraniec B, Frackowiak E, Szostak K, Béguin F. *In vitro* studies of carbon nanotubes biocompatibility. Carbon 2006; 44:1106-1111.
9) Lovat V, Pantarotto D, Lagostena L, Cacciari B, Grandolfo M, Righi M, Spalluto G, Prato M, Ballerini L. Carbon nanotube substrates boost neuronal electrical signaling. Nano Lett 2005; 5:1107-1110.
10) Tian F, Cui D, Schwarz H, Estrada GG, Kobayashi H. Cytotoxicity of single-wall carbon nanotubes on human fibroblasts. Toxicol *In Vitro* 2006; 20:1202-1212.
11) Bottini M, Bruckner S, Nika K, Bottini N, Bellucci S, Magrini A, Bergamaschi A, Mustelin T. Multi-walled carbon nanotubes induce T lymphocyte apoptosis. Toxicol Lett 2006; 160:121-126.
12) Monteiro-Riviere NA, Nemanich RJ, Inman AO, Wang YY, Riviere JE. Multi-walled carbon nanotube interactions with human epidermal keratinocytes. Toxicol Lett 2005; 155:377-384.
13) Cui D, Tian F, Ozkan CS, Wang M, Gao H. Effect of single wall carbon nanotubes on human HEK293 cells. Toxicol Lett 2005; 155:73-85.
14) Yokoyama A, Sato Y, Nodasaka Y, Yamamoto S, Kawasaki T, Shindoh M, Kohgo T, Akasaka T, Uo M, Watari F, Tohji K. Biological behavior of hat-stacked carbon nanofibers in the subcutaneous tissue in rats. Nano Lett 2005; 5:157-161.
15) Wang W, Omori M, Watari F, Yokoyama A. Novel bulk carbon nanotube materials for implant by spark plasma sintering. Dent Mater J 2005; 24:478-486.
16) Aoki N, Yokoyama A, Nodasaka Y, Akasaka T, Uo M, Sato Y, Tohji K, Watari F. Cell culture on a carbon nanotube scaffold. J Biomed Nanotechnol 2005; 1:402-405.
17) Aoki N, Yokoyama A, Nodasaka Y, Akasaka T, Uo M, Sato Y, Tohji K, Watari F. Strikingly extended morphology of cells grown on carbon nanotubes. Chem Lett 2006; 35:508-509.
18) Langer R, Vacanti JP. Tissue engineering. Science 1993; 260:920-926.
19) Desai TA. Micro- and nanoscale structures for tissue engineering constructs. Med Eng Phy 2000; 22:595-606.
20) Zanello LP, Zhao B, Hu H, Haddon RC. Bone cell proliferation on carbon nanotubes. Nano Lett 2006; 6:562-568.
21) Olivier V, Faucheux N, Hardouin P. Biomaterial challenges and approaches to stem cell use in bone reconstructive surgery. DDT 2004; 9:803-811.
22) Sachlos E, Czernuszka JT. Making tissue engineering scaffolds work. Eur Cells Mater 2003; 5:29-39.
23) Correa-Duarte MA, Wagner N, Rojas-Chapana J, Morsczeck C, Thie M, Giersig M. Fabrication and biocompatibility of carbon nanotube-based 3D networks as scaffolds for cell seeding and growth. Nano Lett 2004; 4:2233-2236.
24) Mattson MP, Haddon RC, Rao AM. Molecular functionalization of carbon nanotubes and use as substrates for neuronal growth. J Mol Neurosci 2000; 14:175-182.
25) Webster TJ, Waid MC, McKenzie JL, Price RL, Ejiofor JU. Nano-biotechnology: carbon nanofibers as improved neural and orthopedic implants. Nanotechnology 2004; 15:48-54.
26) MacDonald RA, Laurenzi BF, Viswanathan G, Ajayan PM, Stegemann JP. Collagen-carbon nanotube composite materials as scaffolds in tissue engineering. J Biomed Mater Res A 2005; 74:489-496.
27) Sato Y, Yokoyama A, Shibata K, Akimoto Y, Ogino S, Nodasaka Y, Kohgo T, Tamura K, Akasaka T, Uo M, Motomiya K, Jeyadevan B, Ishiguro M, Hatakeyama R, Watari F, Tohji K. Influence of length on cytotoxicity of multi-walled carbon nanotubes against human acute monocytic leukemia cell line THP-1 *in vitro* and subcutaneous tissue of rats *in vivo*. Mol Biosyst 2005; 1:176-182.
28) Watari F, Yokoyama A, Omori M, Hirai T, Kondo H, Uo M, Kawasaki T. Biocompatibility of materials and development to functionally graded implant for bio-medical application. Compos Sci Technol 2004; 64:893-908.
29) Yuda A, Ban S, Izumi Y. Biocompatibility of apatite-coated titanium mesh prepared by hydrothermal-electrochemical method. Dent Mater J 2005; 24:588-595.
30) Anselme K. Osteoblast adhesion on biomaterials. Biomaterials 2000; 21:667-681.
31) Deligianni DD, Katsala ND, Koutsoukos PG, Missirlis YF. Effect of surface roughness of hydroxyapatite on human bone marrow cell adhesion, proliferation, differentiation and detachment strength. Biomaterials 2000; 22:87-96.
32) Popat KC, Leary Swan EE, Mukhatyar V, Chatvanichkul KI, Mor GK, Grimes CA, Desai TA. Influence of nanoporous alumina membranes on long-term osteoblast response. Biomaterials 2005; 26:4516-4522.
33) Akasaka T, Watari F. Nano-architecture on carbon nanotube surface by biomimetic coating. Chem Lett 2005; 34:826-827.
34) Bianco A, Kostarelos K, Prato M. Applications of carbon nanotubes in drug delivery. Curr Opin Chem Biol 2005; 9:674-679.
35) Milligan HL, Davis JW, Edmark KW. The search for

the nonthrombogenic property of colloidal graphite. J Biomed Mater Res 1970; 4:121-138.
36) Delmas PD. Clinical use of biochemical markers of bone remodeling in osteoporosis. Bone 1992; 13:S17-S21.
37) St-Pierre JP, Gauthier M, Lefebvre LP, Tabrizian M. Three-dimensional growth of differentiating MC3T3-E1 pre-osteoblasts on porous titanium scaffolds. Biomaterials 2005; 26:7319-7328.

Development of a 3D Collagen Scaffold Coated With Multiwalled Carbon Nanotubes

AQ2 **Eri Hirata, Motohiro Uo, Hiroko Takita, Tsukasa Akasaka, Fumio Watari, Atsuro Yokoyama**

Department of Oral Functional Science, Graduate School of Dental Medicine, Hokkaido University, Kita-ku, Sappro 060-8586, Japan

Received 9 July 2008; revised 21 October 2008; accepted 2 December 2008
Published online 00 Month 2009 in Wiley InterScience (www.interscience.wiley.com). DOI: 10.1002/jbm.b.31327

Abstract: Carbon nanotubes (CNTs) have attractive biochemical properties such as strong cell adhesion and protein absorption, which are very useful for a cell cultivation scaffold. In this study, we prepared a multiwalled carbon nanotube-coated collagen sponge (MWCNT-coated sponge) to improve the surface properties of the collagen sponge, and its cell culturing properties were examined. The suface of the collagen sponge was homogeneously coated with MWCNTs by dispersion. MC3T3-E1 cells were cultured on and inside the MWCNT-coated sponge. The DNA content on the MWCNT-coated sponge after 1 week of culture was significantly higher than on an uncoated collagen sponge ($p < 0.05$). There was no significant difference between the estimated ALP activity normalized by DNA quantity on the MWCNT-coated sponge and that on the uncoated collagen sponge which is well known as one of the best scaffolds for cell cultivation. In addition, the MWCNT-coated surface shows strong cell adhesion. Therefore, the MWCNT-coated collagen sponge is expected to be a useful 3D scaffold for cell cultivation. © 2009 Wiley Periodicals, Inc. J Biomed Mater Res Part B: Appl Biomater 00B: 000–000, 2009

Keywords: carbon nanotubes; coating; collagen sponge honeycomb; 3D scaffolds; cell culture

INTRODUCTION

Carbon nanotubes (CNTs) have high chemical stability, and biochemical properties such as strong cell adhesion,[1] protein absorption[2] and cell differentiation.[3] Favorable biocompatibility *in vivo* was also reported.[4] Therefore, CNTs have been employed for use as a cell culture scaffold in the form of CNT sheets[2] and in composite with collagen[5] or polymers.[6]

On the other hand, for regeneration of more complicated tissues such as bone, a three-dimensional (3D) scaffold is needed. The required properties in addition to the 3D scaffold are biocompatibility, 3D cell proliferation and cell differentiation. Thus, CNTs would be useful as the substrate of a 3D scaffold. Currently, collagen sponges are widely used as 3D scaffolds because of their high biocompatibility. Therefore, CNT coating on the collagen sponge surface could improve its utility as a 3D scaffold.

In this study, multiwalled carbon nanotubes (MWCNTs) were used to coat the surface of a collagen sponge honeycomb to improve its surface properties, and the cell attachment and proliferation in the early term were estimated.

EXPERIMENTAL PROCEDURES

Preparation of MWCNT-coated Sponge

Multiwalled carbon nanotubes (MWCNTs; 20–50 nm in diameter, CNTs, Korea) were carboxylated by the reported method[7] and dispersed in 1 w/v % sodium cholate solution to form a 100 ppm MWCNT suspension. A collagen sponge honeycomb (AteloCell® 3 × 3 × 2 mm^3 in size, pore size 200–400 μm, Koken, Japan) was soaked in the MWCNT suspension for 1 h under gentle shaking and then rinsed with phosphate-buffered saline(PBS; Gibco, USA). The obtained MWCNT-coated collagen sponge (MWCNT-coated sponge) was observed by scanning electron microscopy(SEM; S4000, Hitachi, Japan). The specific resistance of each scaffold was also measured using a digital multimeter (type175, Fluke, USA).

Cell Culture

Mouse osteoblast MC3T3-E1 cells were suspended at 3.0 × 10^4 cells/mL in minimum essential medium, alpha modification (α-MEM; Gibco, USA), containing 10% fetal bovine serum (FBS; Biowest, USA) and 1% penicillin/

Correspondence to: E. Hirata (e-mail: erieri@den.hokudai.ac.jp)
Contract grant sponsor: Ministry of Education, Science, Culture and Sport of Japan; contract grant number: 19390488

J_ID: Z8H Customer A_ID: 08-0374.R2 Cadmus Art: JBMB 31327 Date: 23-JANUARY-09 Stage: I Page: 2

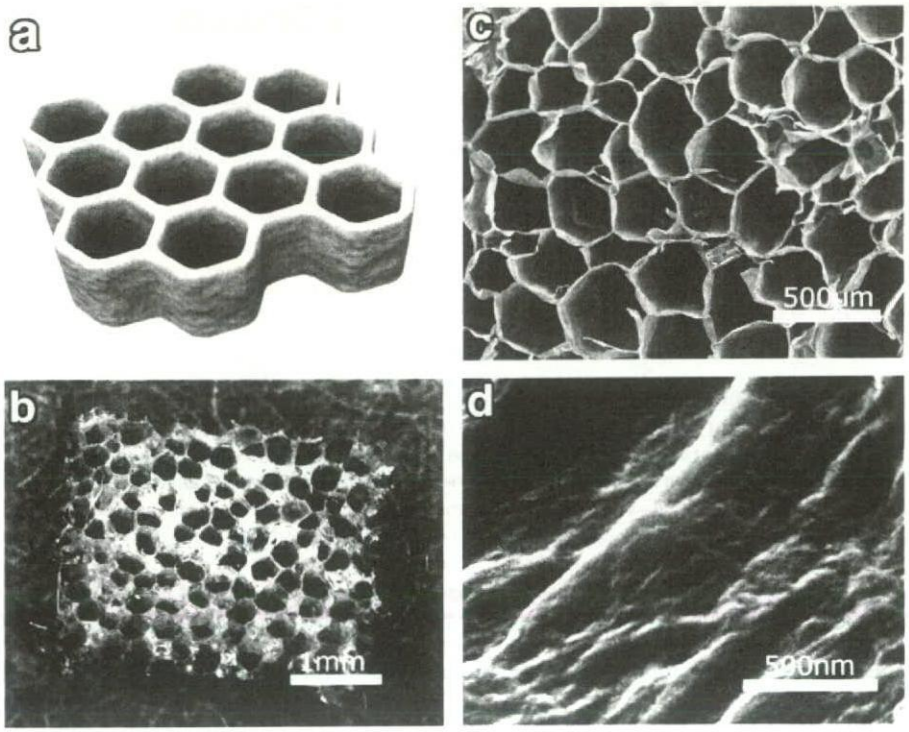

Figure 1. The collagen sponge honeycomb: (a) a schematic model, (b) the whole shape of the collagen sponge, (c)–(d) SEM images of the collagen sponge, (c) at lower magnification, and (d) at higher magnification.

streptomycin. Collagen and MWCNT-coated collagen sponges were placed in the wells of a 96-well plate, and 50 μL of the cell suspension was seeded on scaffold in the wells and then incubated for 7, 14 or 21 days at 37 C in a 5% CO_2 atmosphere.

Cell Morphology

After 7 days of cell culture, the samples were examined biochemically and observed by SEM and optical microscopy. The samples were washed twice with PBS and fixed with 2% glutaraldehyde. After dehydration through a graded series of water-ethanol, half of the samples were freeze-dried and sputter-coated with palladium-platinum for SEM observation. The others were embedded in paraffin and HE-stained for optical microscopic observation. The cell surface morphology was observed by SEM. The cell proliferation on the internal part of the scaffold was observed by optical microscopy.

DNA Quantification and ALP Activity

After 14 or 21 days of cell culture, the amounts of DNA and ALP activities of the samples were measured. The samples were washed twice with PBS. One hundred microliters of the cell suspension containing 0.2% IGEPAL CA-630 (Sigma-Aldrich), 10 m*M* Tris-HCl and 1 m*M* $MgCl_2$, pH 7.4 was added to each sample. The samples were frozen, thawed and homogenized. The sample solution was then shaken for 30 min and centrifuged.

Picogreen (Molecular Probes, Leiden, The Netherlands) was used to measure DNA content. Thirty microliters of the supernatant fluid in the sample gathered with 70 μL of TE buffer was added to 100 mL of picogreen working solution and incubated for 10 min at room temperature in the dark. After incubation, DNA was measured using a fluorometer (F-3000, Hitachi, Japan) with the excitation filter set at 365 nm and the emission filter at 450 nm. A DNA standard curve was made with Lamda DNA.

Alkaline phosphatase (ALP) activity was measured with LabAssay (Wako, Japan). Twenty microliters of the supernatant fluid in the sample was added to 100 μL of *p*-nitrophenol phosphate in carbonate buffer and incubated for 15 min at 37 C. After 80 μL of NaOH was added, absorbance was measured at 405 nm using a plate analyzer (ETY-300, TOYO, Japan) and enzyme activity was determined from the calibration curve of the *p*-nitrophenol standard. ALP activity was normalized by DNA content.

DNA content and ALP activity were determined in four samples and expressed as means ± standard deviations. Data for these measurements were analyzed with Student's two-tailed *t*-test, assuming equal variance, using Microsoft Excel. Statistically significant values were defined as $p < 0.05$.

ID: ananda Date: 23/1/09 Time: 15:25 Path: J:/Production/JBMB/Vol00000/080329/3B2/C2JBMB080329

RESULTS

Scaffold Morphology

F1 Figure 1 shows the shape and the upper surface of a collagen sponge honeycomb. The pore size of the scaffold was 100–400 μm and the pores were longitudinally connected from the top to the bottom surfaces. The surface structure was smooth.

F2 Figure 2 shows the shape and the surface of an MWCNT-coated sponge. The whole shape and honeycomb structure of the collagen sponge were stable after MWCNT coating, as shown in Figure 2(a,c). Figure 2(b) shows the raw MWCNTs. The sponge surface was homogeneously covered by MWCNTs as shown in Figure 2(d) and no aggregation of MWCNTs was observed. The MWCNT-coated sponge showed electron conductivity and the specific resistance was estimated to be 8×10^3 Ωm, but the resistance of the collagen sponge could not be measured because it was over the detection limit (40 MΩ) of the digital multimeter.

Cell Morphology

F3 Figure 3 shows optical microscope images after 1-week incubation. The HE-stained paraffin-embedded specimens were sliced as shown in 3a. The cells covered and spread on the internal sidewall of the CNT-coated sponge as shown in Figure 3(c,d), whereas few cells were observed in the collagen sponge shown in Figure 3(b). Figure 4 shows SEM images of the cells after 1-week incubation. The cells attached to the surfaces of both scaffolds as shown in Figure 4(a,c). However, at higher magnification, the filopodia on the MWCNT net shown in Figure 4(d) were distinct from those on the collagen sponge shown in Figure 4(b). F4

Cell Proliferation and Differentiation

The DNA content and ALP activity of the cells cultivated for 14 or 21 days on the sponges are shown in Figure 5. F5 After 7 days of culture the ALP activities of the cells on both scaffolds were lower than the detection limit of the assay kit used. The DNA content in the cells attached to the MWCNT-coated sponges was significantly higher than that on the uncoated collagen sponges ($p < 0.05$). There was no significant difference between the scaffolds for ALP activity and ALP activity normalized by DNA content at $p > 0.1$.

DISCUSSION

In this study, a surface-modified collagen sponge using MWCNTs was prepared. The surface of the MWCNT-coated sponge was homogeneously covered with MWCNTs using carboxylated MWCNT dispersion with a surfactant.

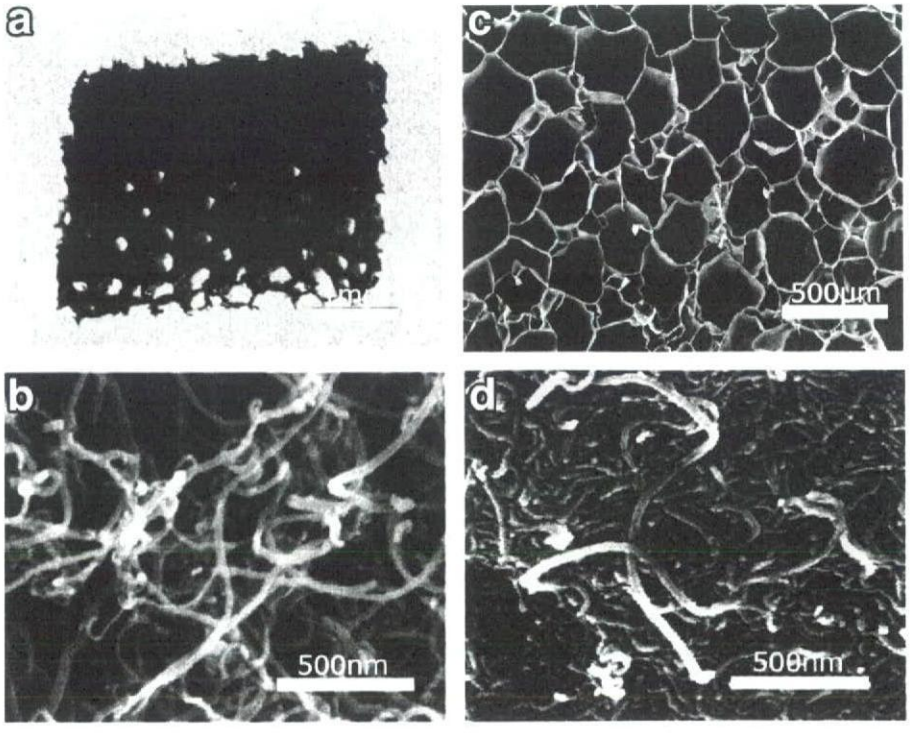

Figure 2. The MWCNT-coated sponge: (a) the whole shape of the MWCNT-coated sponge, (b) SEM image of untreated MWCNTs, (c)–(d) SEM images of the MWCNT-coated sponge, (c) at lower magnification, and (d) at higher magnification.

J_ID: Z8H Customer A_ID: 08-0374.R2 Cadmus Art: JBMB 31327 Date: 23-JANUARY-09 Stage: I Page: 4

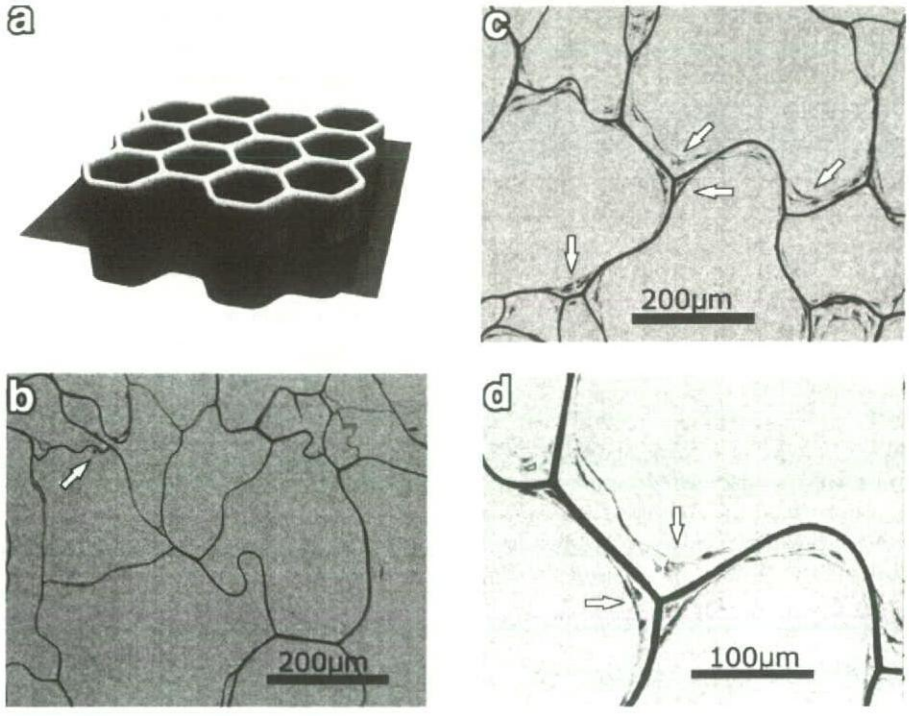

Figure 3. Optical microscopic observation after 1 week of culture: (a) paraffin-embedded specimens were sliced as in the schematic model (b) Few cells are observed in the collagen sponge. (c) Many cells are observed in the MWCNT-coated sponge at low magnification. (d) The cells spread on the sidewall of the MWCNT-coated sponge. [Color figure can be viewed in the online issue, which is available at www.interscience.wiley.com.]

AQ3

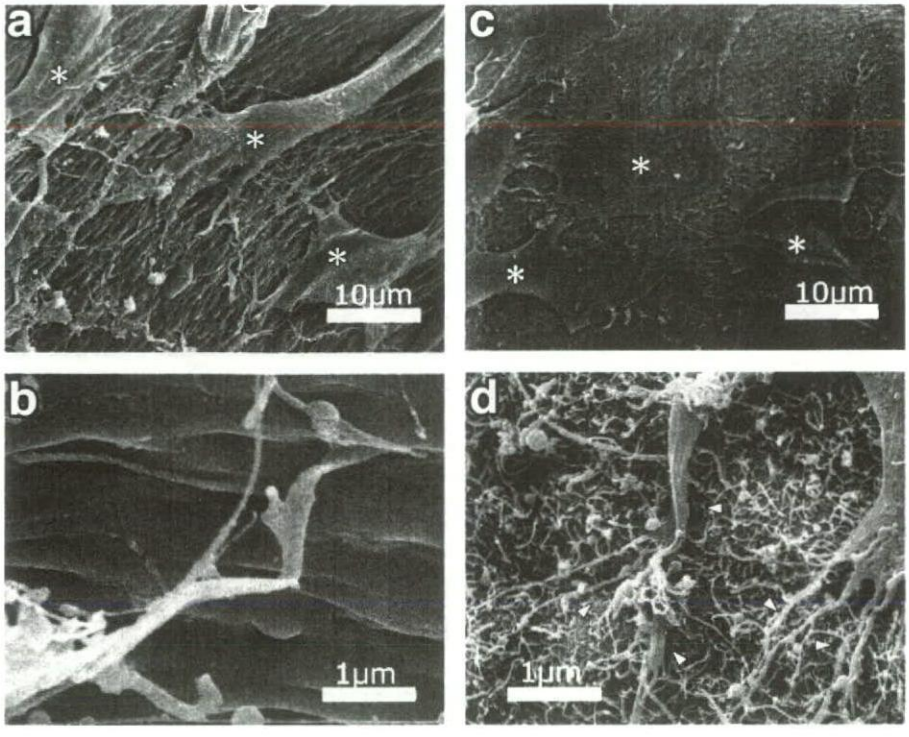

Figure 4. SEM observation after 1-week incubation: cells (asterisk) grown on the (a) collagen sponge and (c) MWCNT-coated sponge. SEM images at higher magnification: (b) collagen sponge, (d) cytoplasmic elongations (arrowhead) intertwined with MWCNTs on the surface of the MWCNT-coated sponge.

ID: ananda Date: 23/1/09 Time: 15:25 Path: J:/Production/JBMB/Vol00000/080329/3B2/C2JBMB080329

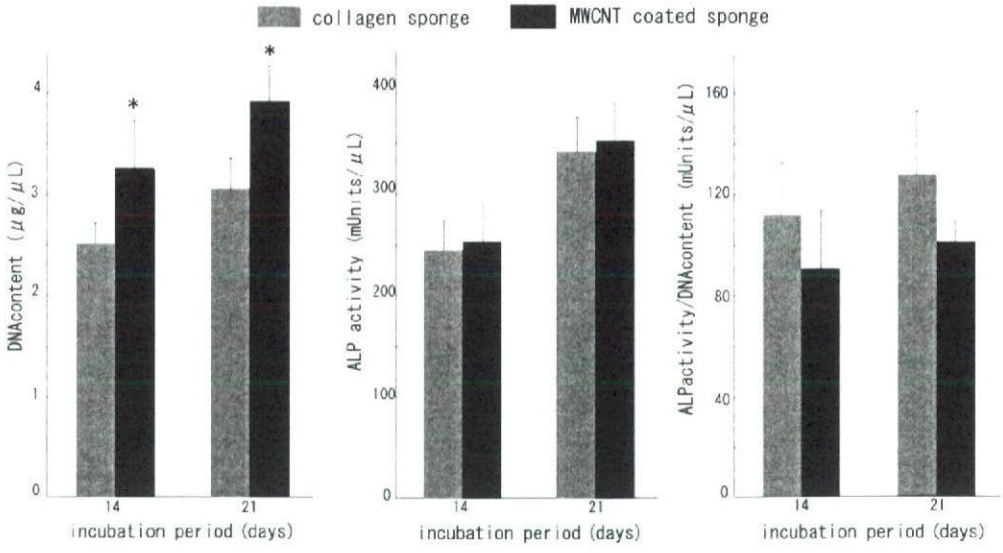

Figure 5. DNA content (left) of the cells cultured on the collagen sponges and MWCNT-coated sponges for 2 and 3 weeks; $n = 4$. The asterisk indicates a statistically significant difference between two scaffold groups (t-test: $p < 0.05$). There were no significant differences between the scaffolds for ALP activity (middle) and ALP/DNA (right).

In Figure 3(c), it can be seen that a large number of cells attached to the internal sidewall of the collagen sponge. The sidewall of the collagen sponge is vertical; thus, it is normally difficult for cells to attach to it. However, MWCNT coating increased the initial cell attachment to the sidewall. One of the reasons for the high cell attachment was suggested to be the mechanical contact between cells and MWCNTs, as can be seen in Figure 4(d), which shows the filopodia of a cell that appear to be twisted around the MWCNTs.

The DNA content of the cells attached to the CNT-coated sponge was significantly higher than that on the uncoated sponge. Usually, DNA content is in proportion to the cell population. Thus, MWCNT coating improved the initial cell attachment to the collagen sponge and assisted proliferation during culture. In a previous study, one of the authors demonstrated that cell growth, proliferation and absorption of the protein in serum on a CNT sheet were higher than on a graphite sheet.[2] Higher protein adsorption on carboxylated MWCNTs than on non-treated MWCNTs[8] were also reported. In addition, the surface roughness of the sponge was increased with MWCNTs as shown in Figures 1 and 2. Therefore, the increase in the surface roughness and the adsorption property of the MWCNT coated surface would be effective for the initial cell attachment.

In this study, the collagen sponge honeycomb, which has many straight macropores (~500 μm) and good mechanical strength.[9] was coated with MWCNTs and good osteoblast cell attachment and proliferation were obtained. Shi et al. developed a CNT-based porous scaffold with pore sizes of 80–100 μm from a composite of SWCNTs and a polymer, and good cell attachment and proliferation were demonstrated.[6] However, to employ the 3D scaffold, interconnecting macropores are required to obtain cell proliferation toward the internal pores. The MWCNT-coating on the collagen sponge honeycomb improved the cell attachment on the internal pore surface as shown in Figure 3, then, the homogeneous cell proliferation on both internal and external surface of the MWCNT coated sponge was achieved. In our previous study, new bone formation on the MWCNTs sintered monolith was reported.[10] Furthermore, the MWCNT-coated sponge exhibited electrical conductivity, whereas collagen is nonconductive; thus, MWCNT coating could make possible culture under electrical stimulation. It has already been reported that the stimulation of osteoblasts by electric pulses can accelerate the multistep process of biomineralization *in vitro*.[11] Therefore, the MWCNT-coated sponge would suggest the feasibility of its use as a scaffold for bone regeneration.

CONCLUSIONS

A 3D cell culture scaffold was obtained by homogeneously coating a collagen sponge honeycomb with MWCNTs. The cell attachment to the internal pore surface was improved by the MWCNT coating. Thereby, homogeneous cell proliferation was achieved not only on the sponge face but also on the internal pore surface.

Therefore, the MWCNT-coated collagen sponge is advantageous as a 3D scaffold for cell cultivation and tissue engineering.

REFERENCES

1. Aoki N, Yokoyama A, Nodasaka Y, Akasaka T, Uo M, Sato Y, Tohji K, Watari F. Strikingly extended morphology of

cells grown on carbon nanotubes. Chem Lett 2006;35:508–509.
2. Aoki N, Akasaka T, Watari F, Yokoyama A. Carbon nanotubes as scaffolds for cell culture and effect on cellular functions. Dent Mater J 2007;26:178–185.
3. Zanello LP, Zhao B, Hu H, Haddon RC. Bone cell proliferation on carbon nanotubes. Nano Lett 2006;6:562–567.
4. Yokoyama A, Sato Y, Nodasaka Y, Yamamoto S, Kawasaki T, Shindoh M, Kohgo T, Akasaka T, Uo M, Watari F, Tohji K. Biological behavior of hat-stacked carbon nanofibers in the subcutaneous tissue in rats. Nano Lett 2005;5:157–161.
5. MacDonald RA, Laurenzi F, Viswanathan G, Ajayan PM, Stegemann JP. Collagen-carbon nanotube composite materials as scaffolds in tissue engineering. J Biomed Mater Res A 2005;74A:489–496.
6. Shi X, Sitharaman B, Pham QP, Liang F, Wu K, Billup WE, Wilson LJ, Mikos AG. Fabrication of porous ultra-short single-walled carbon nanotube nanocomposite scaffolds for bone tissue engineering. Biomaterials 2007;28:4078–4090.
7. Peng H, Alemany LB, Margrave JL, Khabashesku VN. Sidewall carboxylic acid functionalization of single-walled carbon nanotubes. J Am Chem Soc 2003;125:15174–15181.
8. Xaojun L, Wei C, Qiwen Z, Liming D. Direct mesurement of interactions between polypeptides and carbon nanotubes. J Phys Chem B 2006;110:12621–12625.
9. Kakudo N, Shimotsuma A, Miyake S, Kushida S, Kusumoto K. Bone Tissue engineering using human adipose-derived stem cells and honeycomb collagen scaffold. J Biomed Mater Res A 2008;84A:191–197.
10. Wang W, Omori M, Watari F, Yokoyama A. Novel bulk carbon nanotube materials for implant by spark plasma sintering. Dent Mater J 2005;24:478–486.
11. Wiesmann H, Hartig M, Stratmann U, Meyer U, Joos U. Electrical stimulation influences of osteoblast-like cells in vitro. Biochimica et Biophysica Acta 2001;1538:28–37.

ELSEVIER

Materials Science and Engineering A 422 (2006) 218–226

MATERIALS SCIENCE & ENGINEERING A

www.elsevier.com/locate/msea

Effects of moisture and dissolved oxygen in methanol and ethanol solutions containing hydrochloric acid on hydrogen absorption and desorption behaviors of Ni–Ti superelastic alloy

Toshio Ogawa [a], Ken'ichi Yokoyama [b,*], Kenzo Asaoka [b], Jun'ichi Sakai [a]

[a] *Department of Materials Science and Engineering, Waseda University, 3-4-1 Okubo, Shinjuku-ku, Tokyo 169-8555, Japan*
[b] *Department of Biomaterials and Bioengineering, Institute of Health Biosciences, The University of Tokushima Graduate School, 3-18-15 Kuramoto-cho, Tokushima 770-8504, Japan*

Received 15 November 2005; received in revised form 1 February 2006; accepted 3 February 2006

Abstract

The effects of moisture (H_2O concentration) and dissolved oxygen in methanol and ethanol solutions containing 0.1% hydrochloric acid (HCl) on hydrogen absorption and desorption behaviors of the Ni–Ti superelastic alloy have been examined by hydrogen thermal desorption analysis. In the methanol solution, the amount of absorbed hydrogen decreases with increasing H_2O concentration. For 5% H_2O, the thermal desorption peak of hydrogen gradually shifts from 400 to 250 °C with immersion time. When the H_2O concentration is higher than 10%, the hydrogen absorption is not observed. Under a deaerated condition, significant dissolution of the specimen due to corrosion is observed; however, the increment in the amount of desorbed hydrogen is not observed. In the ethanol solution, the critical H_2O concentration for hydrogen absorption is approximately 0.8%. For 2% H_2O, the hydrogen absorption is not exhibited, although slight corrosion is observed. The amount of absorbed hydrogen under the deaerated condition is ten times more than that under the aerated condition. The dissolved oxygen varies the hydrogen desorption behavior.

Keywords: Ni–Ti; Hydrogen embrittlement; Corrosion; Methanol solution; Ethanol solution

1. Introduction

We have recently found that the Ni–Ti superelastic alloy absorbs hydrogen through localized corrosion in methanol and ethanol solutions containing 0.1% hydrochloric acid (HCl), thereby causing hydrogen embrittlement [1,2]. Although the scattering of the amount of hydrogen absorbed in the methanol solution is relatively small [1], the occurrence of hydrogen absorption in the ethanol solution varies widely [2]. The origin of the scattering of hydrogen absorption has not been known, but the presence of moisture (H_2O concentration) and/or dissolved oxygen in the solutions is suspected because they affect sensitively the corrosion resistance of titanium and its alloys [3–7].

The presence of H_2O and dissolved oxygen in the methanol solutions produces an inhibiting effect to corrosion, improving the stability of the hydrated oxide film in the case of titanium and its alloys covered with a thin titanium oxide film [3–7]. Hence, it seems that the H_2O concentration and dissolved oxygen affect the hydrogen absorption behavior of the Ni–Ti superelastic alloy, because the surface of the Ni–Ti superelastic alloy is covered with mainly titanium oxide film.

In contrast, in the ethanol solution, no corrosion of titanium and its alloys occurs [3]. Moreover, no effects of H_2O concentration and dissolved oxygen on the stability of titanium oxide film in ethanol solution containing NaCl are observed, except changing of breakdown potential [5]. However, the Ni–Ti superelastic alloy undergoes localized corrosion in the ethanol solution [2]; the hydrogen absorption behavior of the alloy possibly depends on the H_2O concentration and dissolved oxygen. To understanding the hydrogen embrittlement characteristic of the Ni–Ti superelastic alloy in the methanol and ethanol solutions, it is necessary to investigate the effects of the H_2O concentration and dissolved oxygen on the hydrogen absorption behavior. In particular, the minimum critical H_2O concentration needed to

* Corresponding author. Tel.: +81 88 633 7334; fax: +81 88 633 9125.
E-mail address: yokken@dent.tokushima-u.ac.jp (K. Yokoyama).

0921-5093/$ – see front matter © 2006 Elsevier B.V. All rights reserved.
doi:10.1016/j.msea.2006.02.005

avoid hydrogen absorption is important from the standpoint of inhibiting hydrogen embrittlement.

Because the thermal desorption behavior of hydrogen reflects the state of hydrogen (e.g., hydride, trapped in a defect, in solution) or trap sites in the materials, the correlation of the responsible hydrogen for the embrittlement can be clarified [8–15]. The hydrogen desorption of the Ni–Ti superelastic alloy immersed in the methanol solution appeared as a desorption peak at 350–400 °C [1], whereas that in the ethanol solution appeared as two peaks at approximately 150 and 350 °C [2]. Relationships between the hydrogen desorption behavior and the degradation behavior of mechanical properties of the Ni–Ti superelastic alloy immersed in the methanol solution [1] are not always agreement with those in the ethanol solution [2]. In the present situation where the cause of the change of the hydrogen desorption behavior is not clear, it is difficult to predict and analyze the effects of the H_2O concentration and dissolved oxygen in the methanol and ethanol solutions on the hydrogen desorption behavior of the Ni–Ti superelastic alloy. Therefore, for the future analysis of the state of hydrogen or trap sites, the basic data of the hydrogen desorption behavior must be accumulated at the beginning.

The objective of the present study is to investigate effects of H_2O concentration and dissolved oxygen on hydrogen absorption and desorption behaviors of the Ni–Ti superelastic alloy in methanol and ethanol solutions containing 0.1% HCl by hydrogen thermal desorption analysis (TDA).

2. Experimental procedures

2.1. Materials

A commercial Ni–Ti (Ni: 55 mass%, Ti: balance) superelastic alloy wire 0.50 mm in diameter (described previously [2]) was cut into specimens 50 mm in length. Hereafter, percent in this paper means mass percent, unless otherwise stated. The specimens were polished with 600-grit SiC papers and ultrasonically cleaned with acetone for 5 min. The mechanical properties and phase transformation temperatures of the specimen are listed in Table 1, in which M_s and M_f are the start and finish temperatures for martensite transformation, respectively, on cooling. Similarly, A_s and A_f indicate the start and finish temperatures, respectively, for the reverse transformation on heating. The phase transformation temperatures of the specimen were determined by differential scanning calorimetry (DSC) at a scan rate of 10 °C/min. The critical stress for martensite transformation and the tensile strength were measured at room temperature (25 ± 2 °C). Standard deviation was calculated from the results obtained from five specimens.

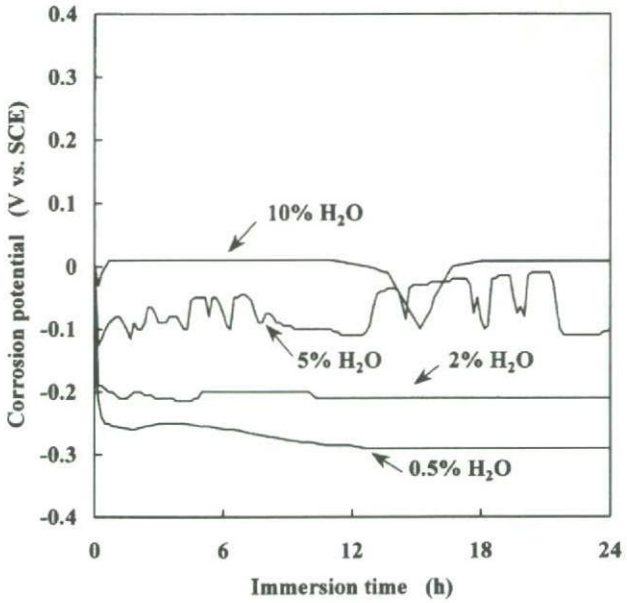

Fig. 1. Changes in corrosion potentials of Ni–Ti superelastic alloy specimens in 0.1% HCl-containing methanol solutions with various H_2O concentrations.

2.2. Test solutions

Chemical-agent-grade methanol or ethanol solutions containing 0.1 mass% HCl were used as the test solutions. These solutions contained initially 0.5 and 0.8 mass% H_2O, respectively. To examine the effects of H_2O, various H_2O concentrations of the test solutions were prepared by adding distilled water. The temperature of the test solutions was kept at 37 ± 0.5 °C.

2.3. Corrosion test

Corrosion potentials of the specimens were measured in 150 ml of the test solutions. The counter and reference electrodes used were a platinum electrode and a saturated calomel electrode (SCE), respectively. To determine the effects of dissolved oxygen concentrations, test solutions exposed to air and deaerated by 99.999% N_2 gas bubbling for 90 min with 190 ml/cm^2 solution were used. The measurements were started 10 s after immersion in the test solutions.

2.4. Immersion test

The specimens were immersed separately in 10 ml of the test solutions for various periods. The mass losses of the immersed specimens with immersion time were measured using a microbalance. The side surfaces of the nonimmersed

Table 1
Mechanical properties and transformation temperatures of tested Ni–Ti superelastic alloy

Critical stress (MPa)	Tensile strength (MPa)	Reduction in area (%)	Transformation temperature (°C)			
			A_f	A_s	M_s	M_f
535 ± 1.4	1425 ± 12.6	54.6	7.5	−26.0	2.5	−38.5

and immersed specimens were observed by scanning electron microscopy (SEM).

2.5. Thermal desorption analysis

The present experimental conditions of TDA were the same as those of our previous studies [1,2]. The amount of desorbed hydrogen was measured by TDA with the specimens subjected to immersion or corrosion tests. Both ends of each specimen (50 mm in length) immersed in the test solution were cut into 20-mm-long segment and subjected to ultrasonic cleaning with acetone for 2 min. The segment was dried in ambient air and used for measurement. TDA was carried out 30 min after the removal of the specimen from the test solution. A quadrupole mass spectrometer (ULVAC, Kanagawa, Japan) was used for the detection of hydrogen. Data sampling was conducted at 30-s intervals at a heating rate of 100 °C/h. The amount of desorbed hydrogen was defined as the integrated peak intensity.

3. Results and discussion

3.1. Effects of H_2O concentration in methanol solution

Fig. 1 shows the effects of the H_2O concentration in methanol solution with 0.1% HCl on the corrosion potential of the Ni–Ti superelastic alloy under the aerated condition. For 0.5% H_2O,

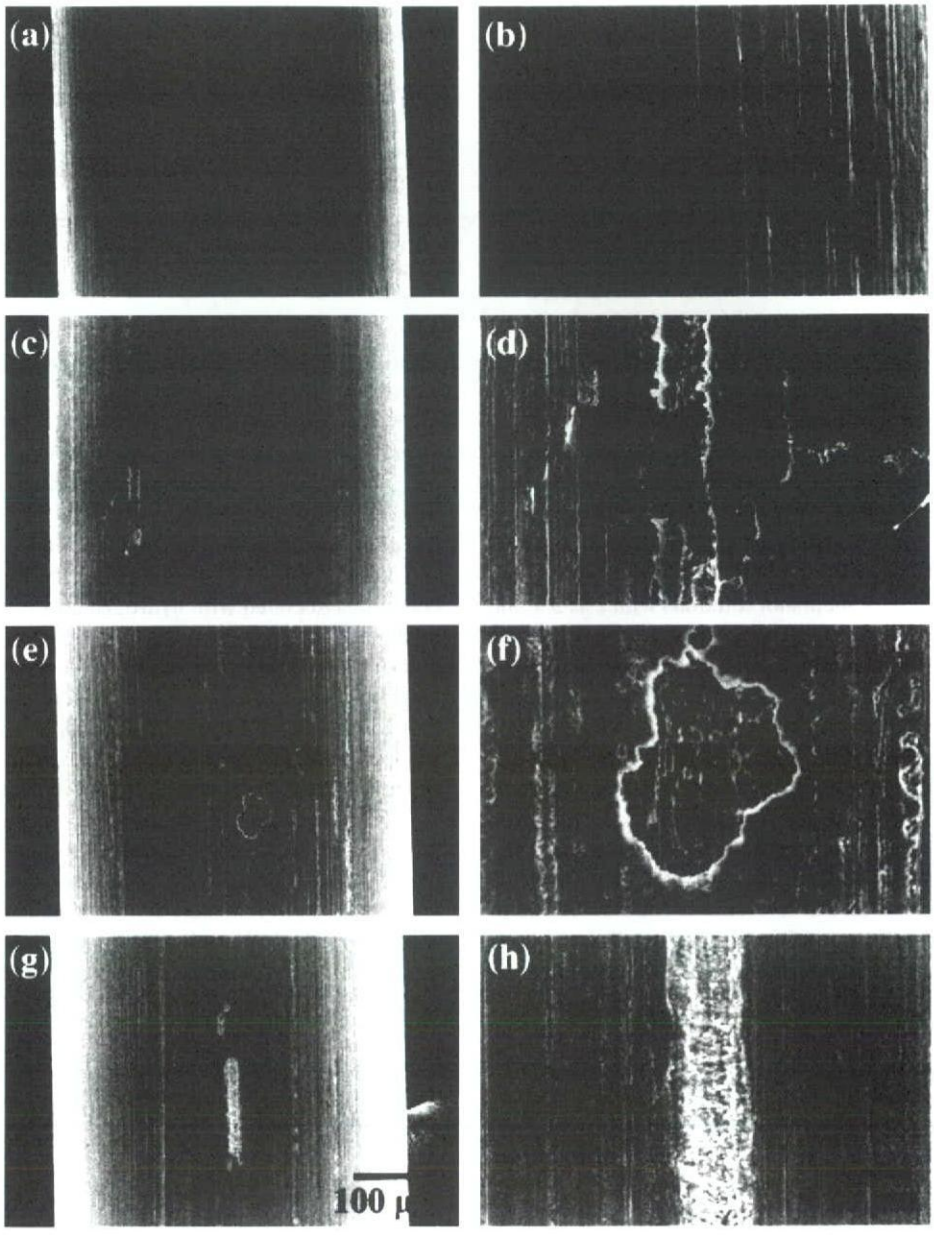

Fig. 2. SEM images of typical side surface: (a) general and (b) magnified views of nonimmersed specimen; (c) general and (d) magnified views of specimen immersed in methanol solution with 2% H_2O for 120 h; (e) general and (f) magnified views of specimen immersed in methanol solution with 5% H_2O for 120 h; and (g) general and (h) magnified views of specimen immersed in methanol solution with 10% H_2O for 120 h.

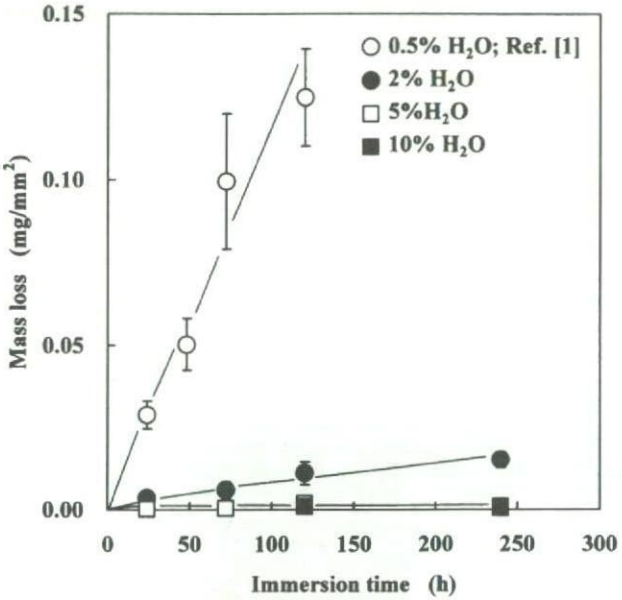

Fig. 3. Mass losses of specimens immersed in methanol solutions with various H_2O concentrations. Standard deviation was calculated from the results of five specimens.

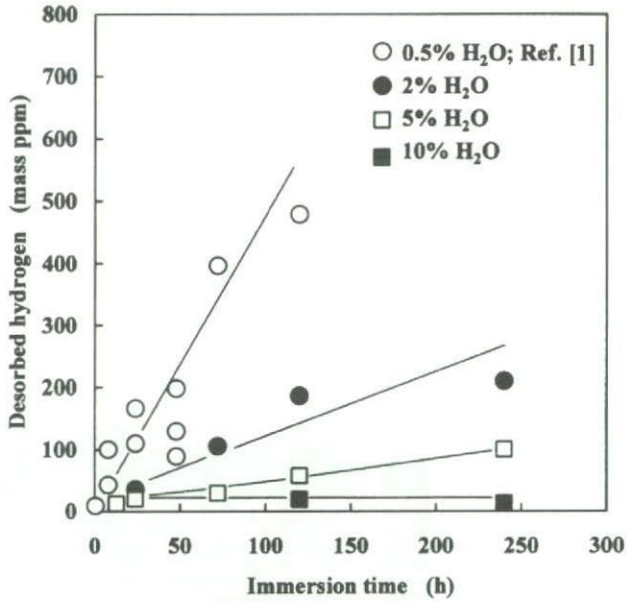

Fig. 4. Amounts of desorbed hydrogen obtained from thermal desorption analysis of specimens immersed in methanol solutions with various H_2O concentrations.

the corrosion potential shifted to the less noble direction immediately after immersion, and then it stabilized at −0.3 V. The corrosion potentials located in the noble direction with increasing H_2O concentration in the methanol solution.

On the side surface of the nonimmersed specimen, scratches due to SiC paper polishing were observed, as shown in Fig. 2(a) and (b). In our previous study [1], a large number of corrosion pits were observed on the surface of the specimen immersed in the methanol solution with 0.5% H_2O. Similarly, localized corrosion was observed for methanol solutions with 2%, 5% and 10% H_2O, as shown in Fig. 2(c)–(h). Corrosion area decreased with increasing H_2O concentration in the methanol solution.

As shown in Fig. 3, the mass losses of the specimens immersed in the methanol solution with 0.5% [1] and 2% H_2O increased with immersion time. The mass loss of the specimen immersed in the methanol solution with 0.5% H_2O was approximately 10 times that with 2% H_2O. When the H_2O concentration in the methanol solution was higher than 5%, the mass loss of the specimen was only slightly detected. These results show that the inhibiting effects of H_2O on the corrosion of the Ni–Ti superelastic alloy are similar to that of titanium and its alloys [3–7] in the methanol solutions. The reason for this is that the titanium hydroxide perhaps forms on the surface of the Ni–Ti superelastic alloy as well as on those of titanium and its alloys, as reported previously [4].

The amounts of desorbed hydrogen of specimens immersed in 0.1% HCl-containing methanol solutions with various H_2O concentrations are shown in Fig. 4. The amount of hydrogen absorbed during the immersion test can be calculated by subtracting the amount of hydrogen desorbed from a nonimmersed specimen, i.e., predissolved hydrogen content of 7 mass ppm, from the total amount of desorbed hydrogen. The amount of absorbed hydrogen increased with immersion time and decreased with increasing H_2O concentration in the methanol solution. For example, upon immersion in the methanol solution with 0.5%, 2% and 5% H_2O for 120 h, the amounts of absorbed hydrogen were approximately 500 [1], 200 and 60 mass ppm, respectively. In the methanol solution with 10% H_2O, the increment in the amount of desorbed hydrogen was not observed irrespective of immersion time. In the case of commercial pure titanium immersed in methanol solution containing 0.4% HCl, an addition of 1.5% H_2O is sufficient to inhibit stress corrosion cracking associated with hydrogen absorption [3,6,16–18]. It is likely that the effects of the H_2O concentration on corrosion and hydrogen absorption prevention in the methanol solution for the Ni–Ti superelastic alloy are one order of magnitude smaller than those for titanium. From Fig. 1, it appears that when the corrosion potential is less noble than approximately −0.1 V, the Ni–Ti superelastic alloy absorbs hydrogen in the methanol solution.

Hydrogen thermal desorption curves from specimens immersed in the 0.1% HCl-containing methanol solution with 2% H_2O are shown in Fig. 5(a). The primary desorption peak appeared at approximately 350 °C and a small secondary peak was observed at approximately 200 °C for an immersion time longer than 72 h. This hydrogen desorption behavior was analogous to that for specimens immersed in the 0.1% HCl-containing methanol solution with 0.5% H_2O, as reported previously [1]. In immersion in the methanol solution with 5% H_2O (Fig. 5(b)), the desorption peak shifted to lower temperature after 120 h, and appeared at approximately 250 °C for the specimen immersed for 240 h.

These results indicate that the H_2O concentration in the methanol solution sometimes affects the hydrogen desorption behavior. The hydrogen desorption behavior provides knowledge regarding the state of hydrogen or trap sites from the desorption profile and the amount of desorption. However, the

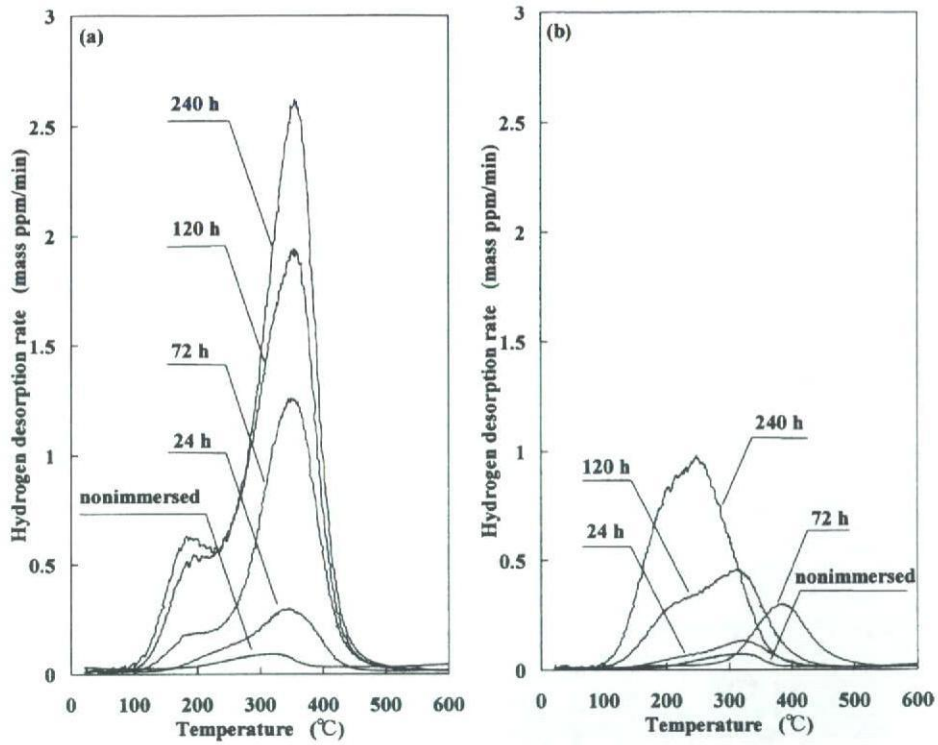

Fig. 5. Hydrogen thermal desorption curves obtained from specimens immersed for various periods in methanol solutions with (a) 2% H_2O and (b) 5% H_2O.

analysis must be performed carefully, because the hydrogen desorption behavior is sometimes influenced by various factors. For example, corrosion products on the surface of the beta titanium alloy often obstruct hydrogen desorption, thereby causing the desorption shift to high temperature [19]. In a separate experiment, we have confirmed that the hydrogen desorption behavior of the Ni–Ti superelastic alloy does not change when the surface of the specimen immersed in the methanol solution is slightly ground using SiC paper. Thus, effects of surface conditions of the specimen on the hydrogen desorption behavior can be neglected in the present study. Moreover, for the Ni–Ti superelastic alloy, the condition of hydrogen absorption often dominates whether hydrides form or not [20–25]. In the present study, hydride formation was not detected by X-ray diffraction (XRD) measurements; most of the absorbed hydrogen probably exists as trapped and/or in solution. Consequently, the change of the hydrogen desorption behavior may be attributed to the change of the state of hydrogen or trap sites, although unknown factors are excluded from the consideration.

3.2. Effects of dissolved oxygen in methanol solution

Fig. 6 shows the corrosion potential of the Ni–Ti superelastic alloy in 0.1% HCl-containing methanol solution with 0.5% H_2O under aerated and deaerated conditions. The potential under the deaerated condition was stabilized at −0.35 V and located in the less noble direction compared with that under the aerated condition.

General corrosion and corrosion products were revealed on the surface of the specimen immersed in the methanol solution for 24 h under the deaerated condition (Fig. 7(a) and (b)), whereas localized corrosion occurred under the aerated condition reported previously [1]. Under the deaerated condition, the diameter of the specimen was reduced from 0.50 to 0.38 mm.

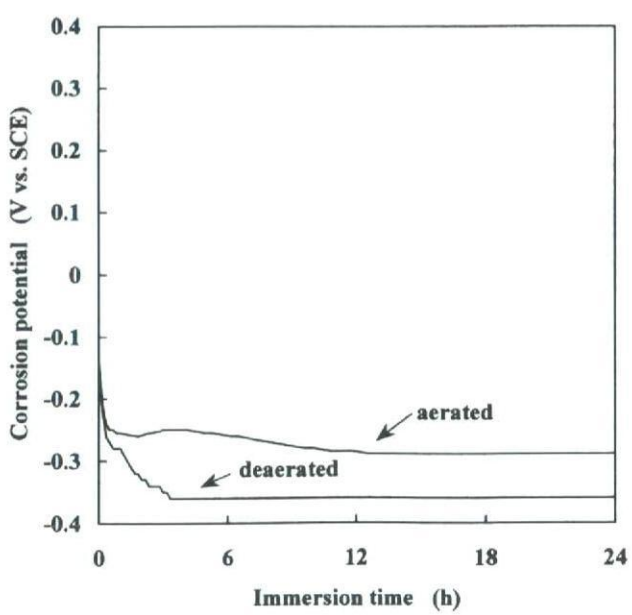

Fig. 6. Changes in corrosion potentials of specimen in methanol solution under aerated and deaerated conditions.

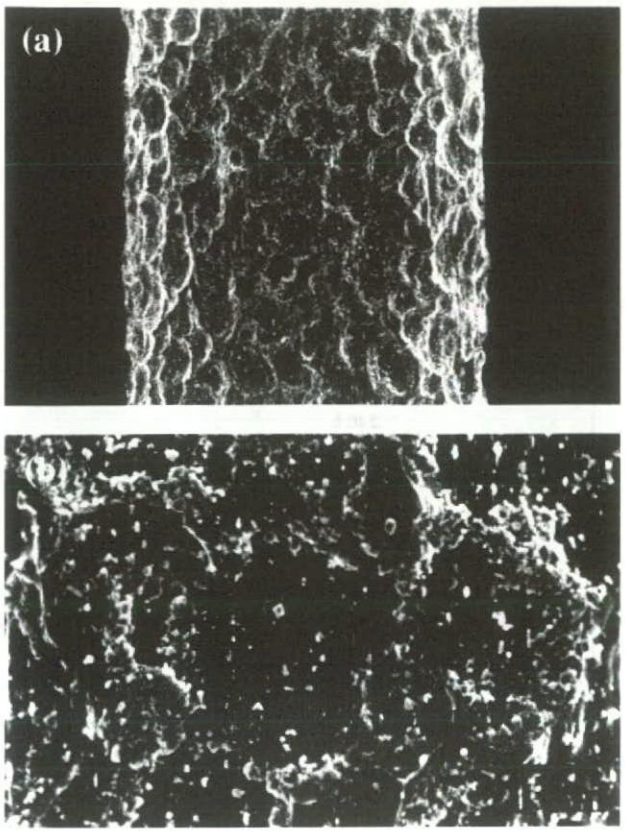

Fig. 7. SEM images of typical side surface of specimen immersed in methanol solution for 24 h under deaerated condition. (a) General and (b) magnified views.

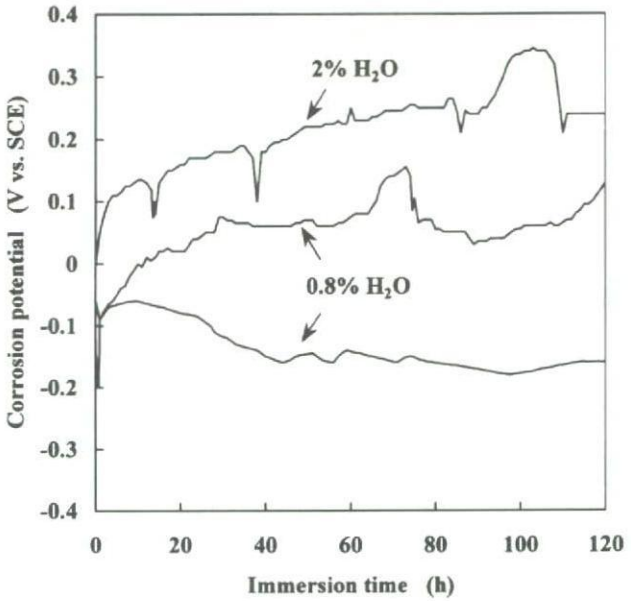

Fig. 8. Changes in corrosion potentials of specimens in ethanol solution with 0.8% and 2% H_2O.

This result indicates that the absence of dissolved oxygen leads to a steep increment in corrosion rate. Conversely, only a slight increment in the amount of desorbed hydrogen was confirmed for the immersed specimen under the deaerated condition. The probable reason for this is that the rate of dissolution due to corrosion of the surface layer of the immersed specimen was larger than the diffusion rate of hydrogen. The diffusion distance of hydrogen in the specimen is calculated to be approximately 50 μm at most for 24 h at 37 °C, using the diffusion coefficient of hydrogen in Ni–Ti alloy with a B2 structure reported by Schmidt et al. [26].

3.3. Effects of H_2O concentration in ethanol solution

Fig. 8 shows the changes in the corrosion potentials of the Ni–Ti superelastic alloy in the 0.1% HCl-containing ethanol solution with 0.8% and 2% H_2O under the aerated condition. For 0.8% H_2O, the corrosion potential varied widely and was classified into two behaviors. One corresponds to the corrosion potential ranging from −0.1 to −0.2 V. In this case, the hydrogen absorption was observed; the hydrogen thermal desorption behavior and the side surface of the immersed specimen subjected to corrosion have been reported in our previous article [2]. The other corresponds to the corrosion potential between −0.1 and 0.1 V. Only a weak hydrogen absorption was confirmed in this potential range. The critical corrosion potential for hydrogen

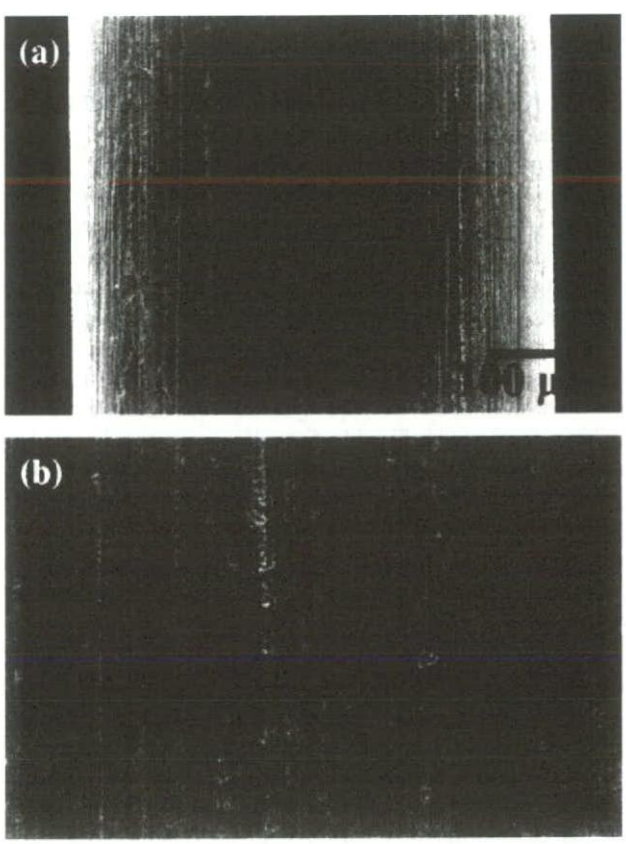

Fig. 9. SEM images of typical side surface of specimen immersed in ethanol solution with 2% H_2O for 120 h. (a) General and (b) magnified views.

absorption, i.e., −0.1 V, in the ethanol solution was consistent with that in the methanol solution. In the case of 2% H_2O, the corrosion potential gradually shifted to the noble direction and reached 0.3 V. As shown in Fig. 9(a) and (b), slight corrosion was observed on the surface of the specimen immersed in ethanol solution with 2% H_2O after 120 h, although mass loss and increment in the amount of desorbed hydrogen were rarely detected. In a separate experiment, we have confirmed that when the specimen is immersed in 0.07% HCl-containing ethanol solution with 0.6% H_2O for 120 h, hydrogen absorption always occurs: the amount of absorbed hydrogen does not scatter (98 ± 7 mass ppm, $n = 5$). These results suggest that the minimum critical H_2O concentration in 0.1% HCl-containing ethanol solution needed to inhibit hydrogen absorption is approximately 0.8%. It is likely that the hydrogen absorption of the Ni–Ti superelastic alloy immersed in the ethanol solution is more susceptible to the H_2O concentration in comparison with that in the methanol solution. Furthermore, the H_2O concentration in the ethanol solution is probably one origin of the scattering of hydrogen absorption reported previously [2].

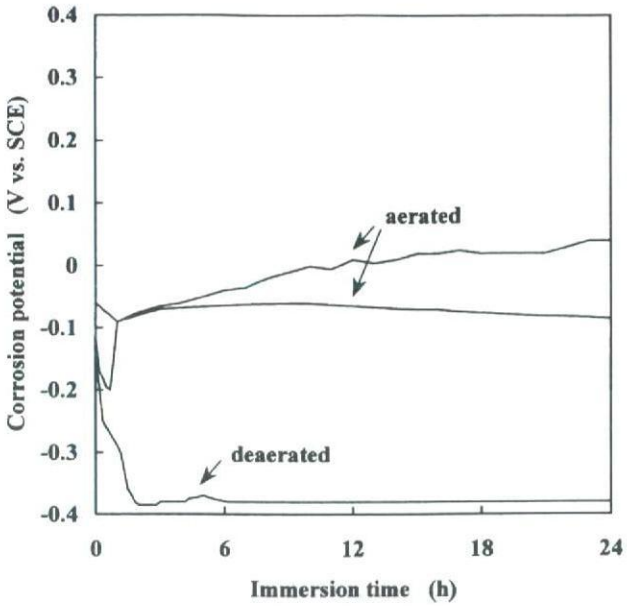

Fig. 10. Changes in corrosion potentials of specimens in ethanol solution under aerated and deaerated conditions.

3.4. Effects of dissolved oxygen in ethanol solution

As shown in Fig. 10, the corrosion potential of the Ni–Ti superelastic alloy was stabilized at approximately −0.38 V without scattering in the 0.1% HCl-containing ethanol solution with 0.8% H_2O under the deaerated condition. The side surfaces of the specimens immersed in the ethanol solution for 24 h under aerated and deaerated conditions are shown in Fig. 11. Under the aerated condition, very slight corrosion was observed (Fig. 11(a) and (b)), whereas under the deaerated condition, general corrosion was observed (Fig. 11(c) and (d)). The corrosion of titanium and its alloys does not always occur in the low-dissolved-oxygen conditions in solutions. For instance, in ethanol solution containing NaCl [5] or in artificial saliva [27], the corrosion resistance of titanium and its alloys does not differ much between aerated and deaerated conditions. Nonetheless, the present results show that the absence of dissolved oxygen markedly reduces the corrosion resistance of the Ni–Ti superelastic alloy in the ethanol solution.

Hydrogen thermal desorption curves from specimens immersed in the 0.1% HCl-containing ethanol solution with 0.8% H_2O after 24 h under aerated and deaerated conditions

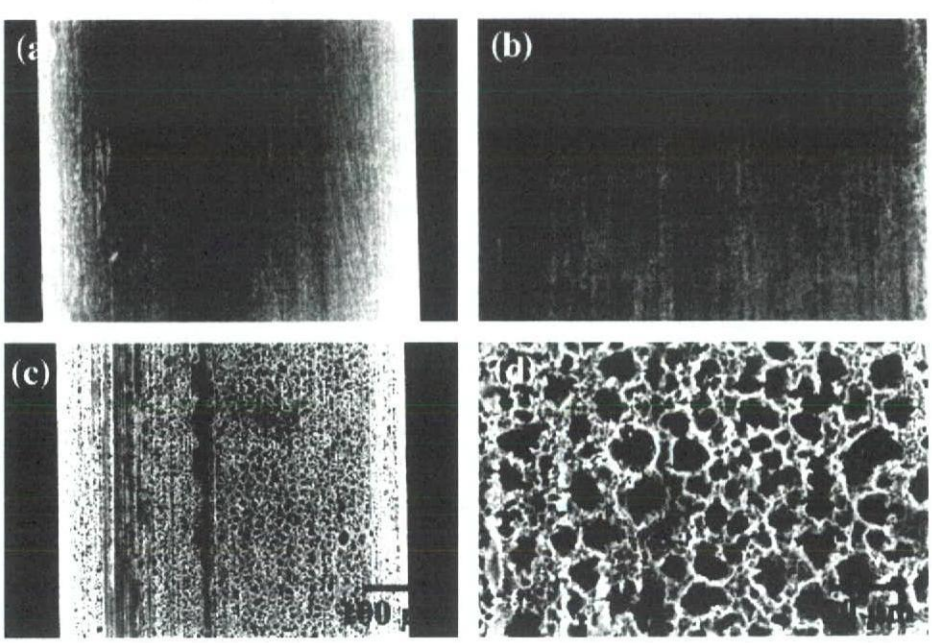

Fig. 11. SEM images of typical side surface: (a) general and (b) magnified views of specimen immersed in ethanol solution 24 h under aerated condition; and (c) general and (d) magnified views of specimen immersed in ethanol solution for 24 h under deaerated condition.

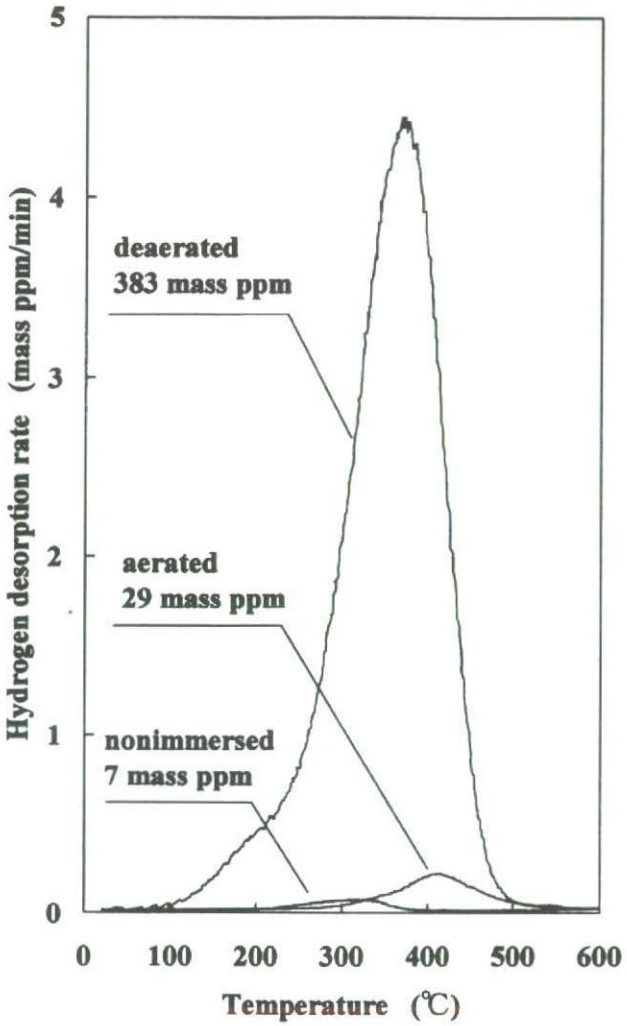

Fig. 12. Hydrogen thermal desorption curves obtained from specimens immersed in ethanol solution for 24 h under aerated and deaerated conditions.

are shown in Fig. 12. Under the deaerated condition, hydrogen absorption always occurred and hydrogen desorption peak appeared at approximately 380 °C. Under the aerated condition, hydrogen desorption peak appeared at approximately 420 °C; however, as the amount of absorbed hydrogen increased, the hydrogen desorption was observed as two peaks at approximately 150 and 350 °C [2]. That is, for the same amount of absorbed hydrogen, the hydrogen desorption behavior differs between aerated and deaerated conditions.

The amount of desorbed hydrogen under the deaerated condition (383 mass ppm) was one order of magnitude larger that under the aerated condition (29 mass ppm). The hydrogen absorption rate, i.e., the amount of absorbed hydrogen per unit time, was extremely enhanced by the absence of dissolved oxygen. The hydrogen absorption rate might affect the hydrogen desorption behavior. Thus, it seems that the absence of dissolved oxygen leads to the increment in the hydrogen absorption rate, thereby changing the hydrogen desorption behavior. However, even if the hydrogen absorption rate is the same, the hydrogen desorption behavior is not necessarily the same [1,2,25,28–30]. Accordingly, the change of the hydrogen desorption behavior may be ascribed to effects of dissolved oxygen itself. In any case, dissolved oxygen changes the hydrogen desorption behavior, namely, the state of hydrogen or trap sites in the Ni–Ti superelastic alloy.

In the ethanol solutions both under aerated and deaerated conditions, hydride formation was not confirmed by XRD measurements. Moreover, from desorbing hydrogen at high temperature, most of the hydrogen absorbed under the deaerated condition is perhaps trapped strongly. The state of hydrogen or trap sites is still being analyzed.

In the present study, it became clear that as causes of changes of the hydrogen absorption and desorption behaviors of the Ni–Ti superelastic alloy immersed in methanol and ethanol solutions containing 0.1% HCl, there are effects of the H_2O concentration and dissolved oxygen. Haruna et al. [31] demonstrated that initiation of environment-assisted cracking of titanium in methanol solution containing $CaCl_2$ is dominated by the concentration of dissociated chloride ion. Usually, HCl is easily dissociated into hydrogen and chloride ions in methanol solution, compared with ethanol solution. This difference of the dissociation behavior of HCl also may affect hydrogen absorption and desorption behaviors.

4. Conclusions

We have demonstrated that H_2O concentration and dissolved oxygen in methanol and ethanol solutions containing 0.1% HCl affect hydrogen absorption and desorption behaviors of the Ni–Ti superelastic alloy. In the methanol solution, for 5% H_2O, the thermal desorption peak shifts to the low-temperature region. Upon adding 10% H_2O to the solution, hydrogen absorption is suppressed. The absence of dissolved oxygen results in the dissolution of the specimen being faster than hydrogen entry into the specimen. In the ethanol solution, the H_2O concentration for the inhibition of hydrogen absorption is above 0.8%. The absence of dissolved oxygen enhances extremely the hydrogen absorption rate and changes the hydrogen thermal desorption to a single peak at approximately 380 °C.

Acknowledgements

This study was supported in part by a Grant-in-Aid for Young Scientists (B) (17791397) and a Grant-in-Aid for Scientific Research (C) (15560632) from the Ministry of Education, Culture, Sports, Science and Technology, Japan.

References

[1] K. Yokoyama, T. Ogawa, K. Asaoka, J. Sakai, M. Nagumo, Mater. Sci. Eng. A 360 (2003) 153.
[2] T. Ogawa, K. Yokoyama, K. Asaoka, J. Sakai, Mater. Sci. Eng. A 393 (2005) 239.
[3] K. Mori, A. Takamura, T. Shimose, Corrosion 22 (1966) 29.
[4] G. Sanderson, J.C. Scully, Corros. Sci. 8 (1968) 541.
[5] A. Cerquetti, F. Mazza, Corros. Sci. 13 (1973) 337.
[6] A.C. Hollis, J.C. Scully, Corros. Sci. 34 (1993) 837.
[7] T. Haruna, M. Yamamoto, T. Shibata, J. Jpn. Inst. Met. 63 (1999) 977.

[8] W.Y. Choo, J.Y. Lee, Metall. Trans. A 13A (1982) 135.
[9] K. Ono, M. Meshii, Acta Metall. Mater. 40 (1992) 1357.
[10] A. Takasaki, Y. Furuya, K. Ojima, Y. Taneda, J. Alloys Compd. 224 (1995) 269.
[11] A. Turnbull, R.B. Hutchings, D.H. Ferriss, Mater. Sci. Eng. A 238 (1997) 317.
[12] S.W. Smith, J.R. Scully, Metall. Mater. Trans. A 31A (2000) 179.
[13] M. Nagumo, M. Nakamura, K. Takai, Metall. Mater. Trans. A 32A (2001) 339.
[14] K. Takai, R. Watanuki, ISIJ Int. 43 (2003) 520.
[15] T. Nishiue, Y. Kaneno, H. Inoue, T. Takasugi, J. Alloys Compd. 364 (2004) 214.
[16] I.A. Menzies, A.F. Averill, Electrochim. Acta 13 (1968) 807.
[17] J.C. Scully, T.A. Adepoju, Corros. Sci. 17 (1977) 789.
[18] K. Ebtehaj, D. Hardie, R.N. Parkins, Corros. Sci. 25 (1985) 415.
[19] T. Ogawa, K. Yokoyama, K. Asaoka, J. Sakai, J. Alloys Compd. 396 (2005) 269.
[20] N. Wade, Y. Adachi, Y. Hosoi, Scripta Metall. Mater. 24 (1990) 1051.
[21] T. Hoshiya, S. Den, H. Katsuta, H. Ando, J. Jpn. Inst. Met. 56 (1992) 747.
[22] T. Asaoka, T. Kamimura, H. Saito, Y. Ishida, J. Jpn. Inst. Met. 56 (1992) 1111.
[23] F.T. Cheng, P. Shi, H.C. Man, Scripta Mater. 47 (2002) 89.
[24] T. Ohba, F. Yanagita, M. Mitsuka, T. Hara, K. Kato, Mater. Trans. 43 (2002) 798.
[25] K. Yokoyama, K. Kaneko, K. Moriyama, K. Asaoka, J. Sakai, M. Nagumo, J. Biomed. Mater. Res. 69A (2004) 105.
[26] R. Schmidt, M. Schlereth, H. Wipf, W. Assmus, M. Müllner, J. Phys. Condens. Matter. 1 (1989) 2473.
[27] M. Nakagawa, S. Matsuya, K. Udoh, Dent. Mater. J. 21 (2002) 83.
[28] K. Yokoyama, S. Watabe, K. Hamada, J. Sakai, K. Asaoka, M. Nagumo, Mater. Sci. Eng. A 341 (2003) 91.
[29] K. Yokoyama, K. Kaneko, K. Moriyama, K. Asaoka, J. Sakai, M. Nagumo, J. Biomed. Mater. Res. 65A (2003) 182.
[30] K. Yokoyama, K. Kaneko, T. Ogawa, K. Moriyama, K. Asaoka, J. Sakai, Biomaterials 26 (2005) 101.
[31] T. Haruna, M. Yamamoto, T. Shibata, J. Jpn. Inst. Met. 63 (1999) 1327.

Photodegradation of Humic Substances on MWCNT/Nanotubular-TiO_2 Composites

Zhiping Zhu,[1,2] Yi Zhou,[2] Hongwen Yu,[1] Tomoko Nomura,[1] and Bunshi Fugetsu*[1,3]
[1]*Graduate School of Environmental Science, Hokkaido University, Sapporo 060-0810*
[2]*Department of Chemistry and Environment Engineering, Changsha University of Science and Technology, Changsha 410076, P. R. China*
[3]*Creative Research Initiative "Souse," Hokkaido University, Sapporo 001-0021*

(Received April 28, 2006; CL-060513; E-mail: hu@ees.hokudai.ac.jp)

We report on the first use of MWCNT/nanotubular-TiO_2 (multiwalled carbon nanotube, MWCNT; TiO_2-derived nanotube, nanotubular-TiO_2) composites as catalysts for photodegradation of aquatic humic substances (HSs). The MWCNT was demonstrated to be capable of enhancing the activity of the photocatalyst. The best degradation efficiency was obtained by using MWCNT/nanotubular-TiO_2 composites having 20% MWCNTs as the photocatalyst.

Elimination of humic substances (HSs) from contaminated water is significant in aquatic system for a number of reasons. First, HSs impart a visible (yellow/brown) color[1,2] to water; this can cause aesthetic contamination even at very low concentrations. Second, HSs are capable of forming complexes with heavy metal ions[3] and/or pollutant organic species[4] (such as pesticides); this can enhanse the absolute solubility and/or the lifetime of these pollutants in water. Moreover, HSs are suspected to be the essential precursors of mutagenic halogenated compounds formed in water after the chlorination.[5,6]

A number of promising techniques have been established for elimination of HSs from the contaminated water. Physical treatment, such as the conventional coagulation/filtration, adsorption and reverse osmosis method offers simpler approaches to the aquatic HSs.[7,8] Chemical and biological elimination methods, on the other hands, also find wide range of applications.[9,10]

Photoelimination, for example, the use of photocatalysts for degrading aquatic HSs, as a typically chemical treatment, is of great interest. However, in case of using titanium dioxide (TiO_2) as the photocatalysts, sufficient amounts of oxygen must be supplied to the reaction system by continuously bubbling the HS/TiO_2 suspension with CO_2-free oxygen.[11]

In this study, we have established a new type of photocatalyst with which aquatic humic substances (HSs) can be degraded without need for oxygen supply. Multiwalled carbon nanotubes (MWCNTs) were coupled with TiO_2-derived nanotubes (nanotubular-TiO_2) to form MWCNT/nanotubular-TiO_2 composite photocatalysts. To our best knowledge, this is the first report dealing with the use of MWCNT/nanotubular-TiO_2 composite photocatalysts for photoelimination of aquatic HSs.

The nanotubular-TiO_2 was prepared using the TiO_2 nanoparticles as the precursory materials. The TiO_2 nanoparticles were obtained by a sol–gel method[12,13] using titanium tetrabutoxide $Ti[O(CH_2)_3CH_3]_4$ as the precursors. The resultant TiO_2 nanoparticles (0.6 g), a certain amount (MWCNT/TiO_2 = 5, 10, 20, and 30 wt %) of highly dispersed MWCNTs (those were obtained by the zwitterionic surfactant dispersion method[14]) were introduced into a Teflon-lined stainless steel autoclave containing 10 M NaOH. This mixture was then heated in an oven at 125 °C for 24 h, similarly to previous reports.[15,16] After being cooled down to room temperature, they were filtrated (Millipore 0.45 μm membrane filter); washed with 0.1 M aqueous HCl solution and then deionized water until its pH value reached to about 7. The products were dried at 105 °C for 6 h and then were calcined at 350 °C for 8 h in ambient atmosphere.

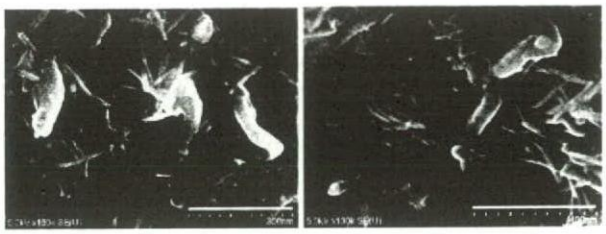

Figure 1. Typical scanning electron microscope (SEM, Hitachi S4800) images of the resultant MWCNT/nanotublar-TiO_2 composites. Bar full size: 300 nm. MWCNTs = 20%.

Scanning electron microcopy (SEM) observations (Figure 1) have demonstrated that the resultant products were consisted of TiO_2-derived nanotubes (nanotubular-TiO_2) together with the highly dispersed MWCNTs. Nanotublar-TiO_2, in general, were built up mainly by amorphous components and hence having poor photocatalysis activities. The MWCNT/nanotubular-TiO_2 composites were further calcined at 350 °C in air, in order to convert nanotubular-TiO_2 into anatase (and hence the higher photocatalysis activities). The successful conversion of the nanotubular-TiO_2 into anatase was demonstrated by XRD analysis of the calcined MWCNT/nanotubular-TiO_2 composites (data not shown). Note that MWNTs disappeared at the calcination temperature higher than 495 °C.

Model aquatic HS solutions (30 mg/L humic acid; pH was adjusted at 4.0 with ammonia and nitric acid solution) were photolyzed in 0.1% suspensions of the resultant MWCNT/nanotubular-TiO_2 composite catalysts using a mercury lamp. Before the mercury lamp was being switched on, the model aquatic HS/MWCNT/nanotubular-TiO_2 solutions were sonicated for 5 min, magnetically stirred in a dark condition for 30 min, in order to achieve the adsorption–desorption equilibrium. This concentration value (C_0) was used as the beginning concentration after the dark adsorption.[17] During the photodegradation, approximately 3 mL samples were withdrawn regularly from the photoreactor (every 30 min or 1 h for each sampling). These samples were filtrated with 0.45 μm Millpore membrane filters and measured using a UV–vis spectrophotometer at 436 and 400 nm (indicating color removal), and 365, 280, and 254 nm (representing TOC normalized aromatic moieties). As can be seen from the typical photodegradation experimental data (Figure 2), the MWCNT/nanotubular-TiO_2 composites provided a better pho-

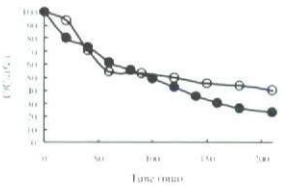

Figure 2. Photodegradation of aquatic humic substances (HSs) with MWCNT/nanotublar-TiO_2 composites (●) and the sole nanotublar-TiO_2 (○) as the photocatalysts. MWCNT = 20%; λ = 254 nm.

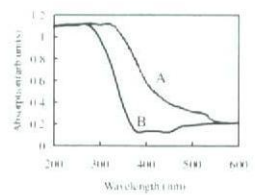

Figure 3. UV–vis absorption spectra of the sole nanotublar-TiO_2 (A) and the MWCNT/nanotublar-TiO_2 composites (B, MWCNT = 20%).

todegradation coefficient than that of the sole nanotubular-TiO_2 for degradation of the aquatic humic substance (HS). Furthermore, for the MWCNT/nanotubular-TiO_2 composites, a significant change (decrease) in concentrations of the aquatic HSs was observed over all the photolyzing process. However, for the nanotubular-TiO_2 alone, it took about an hour to reduce the concentrations of the aquatic HSs by half; after that period of the photolyzation, significant changes of the HS concentrations were not observed.

The synergetic effect of MWCNTs on the photodegradation of the aquatic HSs was found in an order of 20 > 30 > 10 > 5% of the carbon nanotubes in the MWCNT/nanotubular-TiO_2 composites. Namely, the MWCNT/nanotubular-TiO_2 composites with a weight ratio of 20% MWCNTs provided the best synergetic effect on the photodegradation of the aquatic HS.

The diffuse reflectance UV–vis spectra of the MWCNT/nanotubular-TiO_2 composites (Figure 3) gave new insights into the photodegradation mechanism of the MWCNT/nanotubular-TiO_2 composite catalysts. The nanotubular-TiO_2 has showed the characteristic spectrum of anatase with its fundamental absorption edge rising at 400 nm. The MWCNT/nanotubular-TiO_2 composites, on the other hand, have shifted to shorter wavelength. In other words, combining MWCNT with the nanotubular-TiO_2 has resulted a blue shift. It is noticeable that the MWCNT/nanotubular-TiO_2 composites of 20% MWCNTs provided a largest change of the UV–vis spectrum, followed by 30, 10, and then 5%.

MWCNTs are capable of absorbing the irradiation (photons); this results in production of photoinduced electrons over the carbon nanotubes. The photoinduced electrons transferred from MWCNTs into conduction band of the nanotubular-TiO_2. Superoxide radicals (very reactive) formed over the nanotubular-TiO_2 surfaces by transferring the photoinduced electrons into the adsorbed oxygen. Highly reactive hydroxyl radicals might be also formed; in case of formation of positively charged holes by electron migration from the nanotubular-TiO_2 valence band to the carbon nanotubes.[18–20] These resultant radicals are responsible considerably for the degradation of the aquatic humic substances.

Finally, note here that the thermal stability of the MWCNT/nanotubular-TiO_2 composites were investigated using the thermogravimetric method. TG curve indicated mass loss up to 510 °C of a total 21% for the composites containing 20% MWCNTs.

In conclusion, a new type of photocatalysts was established by combination of the TiO_2-derived nanotubes and the highly-dispersed MWCNTs. The nanotubular shapes of TiO_2 provide the desirable morphologies for attaching the photocatalyst onto the sidewalls of the carbon nanotubes. Identification of the main products by analysis of the photolyzed solutions using LC-MS is under investigation.

References

1 A. P. Back, R. F. Christman, *J. Am. Water Works Assoc.* **1963**, *55*, 753.
2 L. E. Bennett, M. Drikas, *Water Res.* **1993**, *27*, 1209.
3 M. Hiraide, Y. Arima, A. Mizuike, *Anal. Chim. Acta* **1987**, *200*, 171.
4 J. F. McCarthy, in *Aquatic Humic Substances: Aquatic Humic Substances: Influence on Fate and Treatment of Pollutants*, ed. by I. H. Suffet and P. MacCarthy, American Chemical Society, Washington, DC, **1989**, p. 263.
5 J. J. Rook, *Water Treat. Exam.* **1974**, *23*, 234.
6 J. J. Rook, *Environ. Sci. Technol.* **1977**, *11*, 478.
7 W. Aui, S. Tamura, M. Abe, K. Ogino, *Sci. Total Environ.* **1992**, *117–118*, 543.
8 C. Jucker, M. M. Clark, *J. Membr. Sci.* **1994**, *97*, 37.
9 J. Zhou, C. J. Banks, *Chemosphere* **1993**, *27*, 607.
10 P. Backlund, *Chemosphere* **1992**, *25*, 1869.
11 R. B. Eggins, F. L. Plalmer, J. A. Byrne, *Water Res.* **1997**, *31*, 1223.
12 X. Liu, J. Yang, L. Wang, X. Yang, L. Lu, X. Wang, *Mater. Sci. Eng. A* **2000**, *289*, 241.
13 G. Colón, M. C. Hidalgo, J. A. Navío, *Catal. Today* **2002**, *76*, 91.
14 B. Fugetsu, W. Han, N. Endo, Y. Kamiya, T. Okuhara, *Chem. Lett.* **2005**, *34*, 1218.
15 T. Kasuga, M. Hiramatsu, A. Hoson, T. Sekino, K. Niihara, *Langmuir* **1998**, *14*, 3160.
16 T. Kasuga, M. Hiramatsu, A. Hoson, T. Sekino, K. Niihara, *Adv. Mater.* **1999**, *11*, 1307.
17 C. S. Uyguner, M. Bekbolet, *Desalination* **2005**, *176*, 167.
18 W. Feng, Y. Feng, Z. Wu, A. Fujii, M. Ozaki, K. Yoshino, *J. Phys.: Condens. Matter* **2005**, *17*, 4361.
19 W. Wang, P. Serp, P. Kalck, J. L. Faria, *J. Mol. Catal. A: Chem.* **2005**, *235*, 194.
20 Y. Yu, J. Yu, J. Yu, Y. Kwok, Y. Che, J. Zhao, L. Ding, W. Ge, P. Wong, *Appl. Catal., A* **2005**, *289*, 186.

Published on the web (Advance View) July 8, 2006; doi:10.1246/cl.2006.890